Journal of Structural Geology 80 (2015) 57–71

Contents lists available at ScienceDirect

Journal of Structural Geology

journal homepage: www.elsevier.com/locate/jsg

Review article

Polymodal faulting: Time for a new angle on shear failure

David Healy [a, *], Thomas G. Blenkinsop [b], Nicholas E. Timms [c], Philip G. Meredith [d], Thomas M. Mitchell [d], Michele L. Cooke [e]

[a] School of Geosciences, University of Aberdeen, Aberdeen AB24 3UE, United Kingdom
[b] School of Earth & Ocean Sciences, Cardiff University, Cardiff CF10 3AT, United Kingdom
[c] Department of Applied Geology, Curtin University, Perth WA 6845, Australia
[d] Department of Earth Sciences, University College, London WC1E 6BT, United Kingdom
[e] Department of Geosciences, University of Massachusetts, Amherst, MA 01003-9297, USA

ARTICLE INFO

Article history:
Received 3 November 2014
Received in revised form
1 July 2015
Accepted 30 August 2015
Available online 3 September 2015

Keywords:
Fault
Pattern
Polymodal
Quadrimodal
Conjugate
Failure

ABSTRACT

Conjugate, or bimodal, fault patterns dominate the geological literature on shear failure. Based on Anderson's (1905) application of the Mohr-Coulomb failure criterion, these patterns have been interpreted from all tectonic regimes, including normal, strike-slip and thrust (reverse) faulting. However, a fundamental limitation of the Mohr-Coulomb failure criterion – and others that assume faults form parallel to the intermediate principal stress, σ_2 – is that only plane strain can result from slip on the conjugate faults. However, deformation in the Earth is widely accepted as being three-dimensional, with truly triaxial stresses ($\sigma_1 > \sigma_2 > \sigma_3$) and strains. Polymodal faulting, with three or more sets of faults forming and slipping simultaneously, can generate three-dimensional strains from truly triaxial stresses. Laboratory experiments and outcrop studies have verified the occurrence of polymodal fault patterns in nature. These fault patterns present a fundamental challenge to our understanding of shear failure in rocks (and other materials) and an opportunity to improve our understanding of seismic hazards and fluid flow in the subsurface. In this review, we assess the published evidence, theories and models for polymodal faulting before suggesting ways to produce a truly general and valid failure criterion for triaxial failure.

Contents

* Corresponding author.
E-mail address: d.healy@abdn.ac.uk (D. Healy).

http://dx.doi.org/10.1016/j.jsg.2015.08.013

1. Introduction

Polymodal fault patterns can be quadrimodal (i.e. four clusters of poles) or display a quasi-continuous orientation distribution of poles spanning finite arcs of strike and dip (Fig. 1; Peacock and Sanderson, 1992 – their Fig. 2). Polymodal fault patterns are therefore distinctly different from the bimodal pattern associated with the better-known case of conjugate faults.

The classical and widely accepted conceptual model for conjugate fault patterns produced by a single homogeneous stress regime dates back to Anderson and his application of the Mohr-Coulomb failure criterion to natural stress states (Anderson, 1905; Jaeger et al., 2009). In that model, two sets of faults (shear fractures) form simultaneously, with the maximum principal stress (σ_1) oriented as their acute bisector, the minimum principal stress (σ_3) bisecting their obtuse angle, and the intermediate principal stress oriented parallel to their mutual intersection (Fig. 1a). On an equal area or equal angle net, conjugate or bimodal fault patterns should appear as two clusters of poles. Allowing for inevitable natural variations in local stresses and local rock properties (such as cohesive strength or friction), one would expect noise in this bimodal orientation distribution, but the pattern should still display two clusters with evidence of central tendency about a mean direction within each of the two clusters.

However, there is significant outcrop-scale field and laboratory-scale experimental evidence for the occurrence of polymodal fault patterns, where three, four or more sets of fault planes have formed and slipped simultaneously. The first laboratory evidence came from the careful and systematic clay-cake experiments of Oertel (1965), which produced four sets of fault planes in response to the applied load. Subsequently, Reches and Dieterich (1983) conducted systematic truly triaxial experiments on small (2.2 cm) cubic samples of sandstone, limestone and granite and produced polymodal fault patterns in all rock types. Ghaffari et al. (2014) and Nasseri et al. (2014) have recently performed truly triaxial tests on larger (8 cm) cubic samples of sandstone and also produced clear evidence of polymodal fault patterns, including novel CT scans of their internal structure and the acoustic emissions produced during their propagation. The first field evidence dates back to Donath (1962) defining a rhombic map pattern in the basalts of the Basin and Range (see also Crider, 2001). Aydin and Reches (1982) reported quadrimodal fault patterns from faulted aeolian sandstones in Utah. Similar patterns have also been measured in sandstones on Arran, Scotland (Woodcock and Underhill, 1987; Underhill and Woodcock, 1987), in the Chalk of northern Germany (Koestler and Ehrmann, 1991), in carbonates of NW Australia (Miller et al., 2007) and in siliciclastics of E Australia (Carvell et al., 2014). All of these accounts describe four sets of contemporaneous faults defining rhombic map patterns or quadrimodal systems, where the poles to the measured fault planes define four clusters on an equal angle net (Fig. 1b and e).

The observation or inference that all four of the fault sets, both

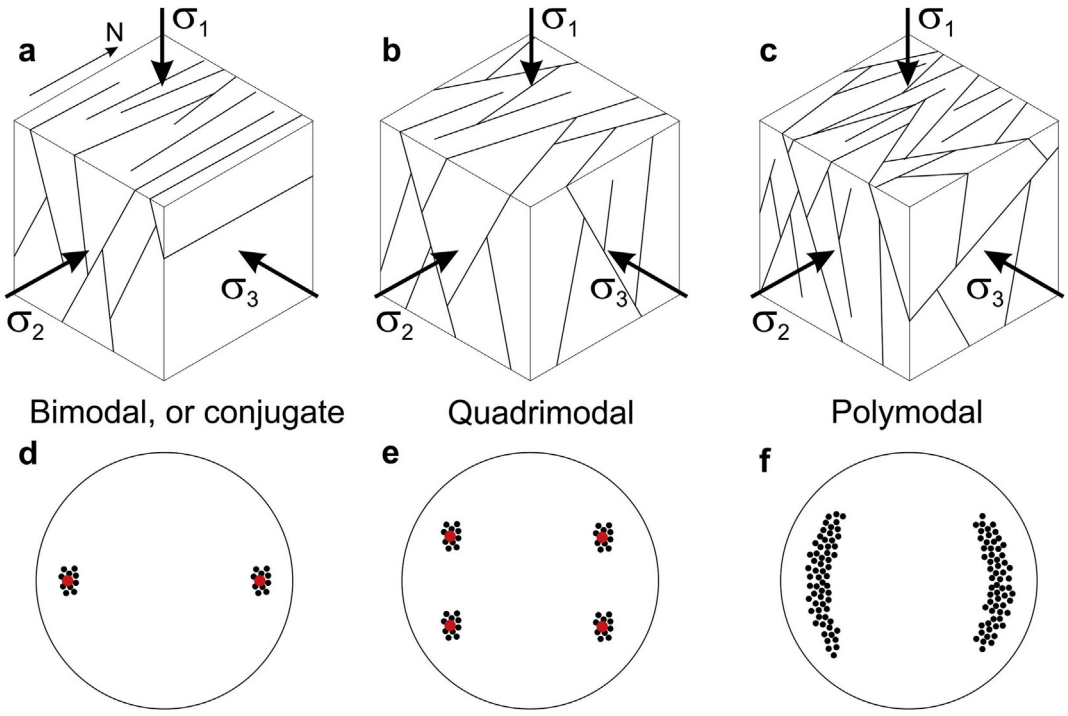

Fig. 1. Schematic block diagrams and equal angle nets showing the difference between a) bimodal (or conjugate), b) quadrimodal and c) polymodal fault patterns. Examples shown are for normal faults with σ_1 vertical. Note that polymodal fault patterns (b, c) are *apparently bimodal or conjugate* on many 2D sections (i.e. faces of the schematic block), and only an equal angle or equal area stereonet of measured 3D orientations shows the true polymodal pattern (compare d), e) and f)). Quadrimodal and polymodal faults are oblique to all three principal stresses. Black dots on the stereographic projections represent poles to faults (shear fractures), and red dots mark the average of each cluster.

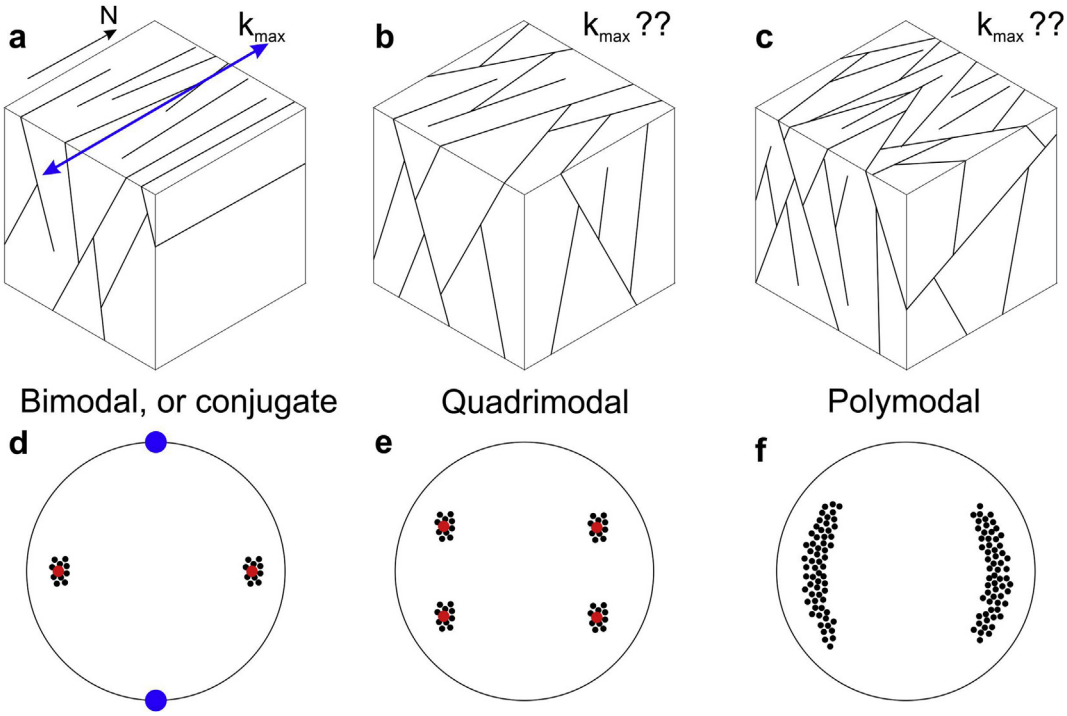

Fig. 2. Equal angle nets showing the influence of fault pattern on the anisotropy of bulk permeability. For bimodal (conjugate) fault patterns, the direction of maximum permeability (k_{max}) is likely to be parallel to the mutual intersections of the faults, shown by the blue arrow in a), and blue dots in d), whether the fault planes are hydraulically sealing or conductive. In the case of quadrimodal and polymodal fault patterns (b, c, e, f) the bulk permeability anisotropy will depend on the hydraulic conductivity of the fault planes – whether they are conduits or barriers – and is likely to be much more complex due to the variability in the orientations of the fault plane intersections.

in the natural field examples and in the laboratory samples, were active simultaneously implies that they formed in response to a single stress regime. Symmetry arguments then lead to the conclusion that all of the fault sets formed and slipped while *oblique* to the direction of the intermediate principal stress (σ_2). This is in contrast to the classical bimodal (conjugate) fault model, where σ_2 lies parallel to the mutual intersection of the two fault sets and plays no role in the failure criterion. The existence of polymodal fault patterns has very significant implications for the mechanics of brittle failure, and in particular, for our ability to accurately predict fault patterns and fault slip from a knowledge of the imposed stress regime.

Wider acceptance of the existence of polymodal fault patterns and a better understanding of the fundamental issues they present is important for a number of reasons. In practical terms, because fracture patterns exert a fundamental control on fluid flow in the subsurface, accurate general models that link principal effective stresses to the orientations of failure planes are always required. An important potential difference between a bimodal (conjugate) fault pattern and a polymodal fault pattern in terms of fluid flow is shown in Fig. 2. Assuming that fault planes are hydraulically sealing, it is clear that a polymodal pattern would result in a strongly compartmentalised fluid reservoir (Fig. 2a and b). In contrast, assuming that fault planes are hydraulically conductive, the greater length of fracture intersections of a polymodal pattern when compared to a bimodal (conjugate) pattern would, in general, produce a higher fluid flow rate (Fig. 2c and d), and in different directions in comparison to a conjugate pattern with the same total number of fault planes. Another approach to fault system permeability is through the connectivity of fault traces or branch lines. Using two dimensional fault trace maps, Manzocchi (2002) and Nixon et al. (2011) have shown the importance of many X (cross-cutting) and Y (splay) nodes for increasing fluid flow through conductive fracture networks. Polymodal fault patterns will, in general, have more X and Y connections in 2D (and more branch lines in 3D) than comparable conjugate (bimodal) patterns. The anisotropy of permeability is therefore expected to be very different in rocks with polymodal fault patterns in comparison to conjugate fault patterns, and this has implications for the development of hydrocarbon reservoirs, the genesis of ore deposits and the management of aquifers.

A more theoretical consideration is that because the orientations of polymodal faults are not predicted by Mohr-Coulomb (or indeed any other) failure criteria, they present a fundamental challenge to our understanding of shear failure in rocks and other materials. The relatively simple difference in geometry between the two kinds of fault pattern – i.e. the orientations of bimodal/conjugate versus polymodal faults – belies the potential significance of understanding how polymodal fault patterns form and then influence fluid flow in the subsurface.

In this paper, we review the evidence for polymodal fault patterns from published examples of outcrop studies and laboratory experiments. We evaluate the models and theories proposed to date to account for their formation, before highlighting the remaining issues and scope for further work. The paper is organised as follows: in the first section we review the field outcrop and map-scale evidence for polymodal fault patterns. We then review laboratory evidence from deformation experiments on both rocks and analogue materials. We subsequently shift focus to the theoretical models that have been proposed to explain the formation of polymodal faults, loosely subdivided into kinematic (or strain-based) and mechanical (or stress-based) models. Following a discussion of the issues presented by these hypotheses and conceptual models, we outline scope for further work before summarising the key points. Throughout the paper, the maximum principal stress is denoted σ_1 and taken as positive in compression, with $\sigma_1 \geq \sigma_2 \geq \sigma_3$.

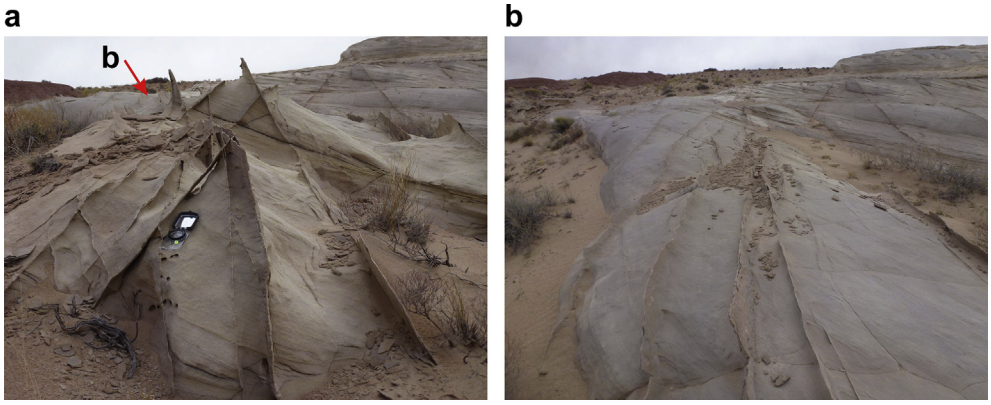

Fig. 3. Photographs of outcrops in Goblin Valley, Utah (USA) showing polymodal deformation bands in dune-bedded aeolian sandstones of the Entrada Formation (see also Aydin and Reches, 1982; their Fig. 3 and 4). The view in a) is approximately a dip section and shows an *apparently* conjugate (bimodal) pattern, intersecting at around 40–50° in this plane (compass-clinometer for scale). The view in b) is an oblique strike section (location shown in a) and shows the same two sets of deformation bands, intersecting at around 40–50° in this plane too.

Principal strains are labelled $\varepsilon_1 \geq \varepsilon_2 \geq \varepsilon_3$, with ε_1 as positive and the largest extension.

2. Field examples

Donath (1962) first described a polymodal fault pattern in Miocene-Pliocene age lavas in southern Oregon (USA), covering an area of about 1000 km^2 (about 22 miles by 19 miles, his Plate 3) in the Basin & Range. Faults exposed at the surface form a rhombic pattern in map view, with two sets of faults striking 325° and 020°, respectively, and intersecting at an angle of 55°. Rose diagrams of measured fault strikes show two broad maxima. Fault dips are steep to sub-vertical at the surface, although most are poorly constrained at depth. Crider (2001) used recent focal mechanisms to infer that these are normal faults dipping between 45° and 80° degrees. Mutually cross-cutting relationships were used to infer that both sets of faults were active at the same time.

The classic example of polymodal fault patterns – and one of many instances featuring high-porosity aeolian sandstones – is from Aydin and Reches (1982). These authors reported examples of fault patterns with orthorhombic symmetry in the Entrada and Navajo sandstones of SE Utah (USA). In their field examples, four sets of faults produce quadrimodal patterns on equal angle nets of poles to planes (Fig. 3). Field evidence of off-setting and cross-cutting among these sets supports the inference that they were contemporaneous. Jamison and Stearns (1982) have also reported polymodal 'microfault' (cataclastic deformation band) patterns from the aeolian Wingate Sandstone in Colorado (USA). Aydin and Reches (1982) make the key point that polymodal fault orientations are not predicted by either the Mohr-Coulomb or Griffith criteria, or by the slip-line theory of plasticity. These theoretical models are only relevant for bulk plane strain, whereas in general geological deformation, strains are expected to be three-dimensional.

This point about 3D strain was taken up by Underhill and Woodcock (1987) and Woodcock and Underhill (1988) in two analyses of cataclastic deformation bands from Arran, Scotland (UK). These deformation bands in Permian aeolian sandstones define quadrimodal patterns of poles on equal angle nets with orthorhombic symmetry. These authors conclude that bimodal Andersonian (or conjugate) fault systems are special cases of plane strain, and that quadrimodal fault systems represent the more general case of triaxial strain. Underhill and Woodcock (1987) make another important point: they use the observation that only small displacements (<10 mm), relative to fault widths, occur on each deformation band as evidence for slip- or strain-hardening behaviour. Deformation band arrays may or may not exhibit strain hardening (see Nicol et al., 2013 for an alternative view) but the small shear strains preserved in these rocks provide a record of the incremental strain, and therefore the geometry of the whole fault pattern can be directly related to the bulk finite strain. The classic study by Krantz (1988) documented in great detail the orthorhombic faults of the Chimney Rock fault array in Utah.

Polymodal fault patterns have been reported from a wide range of lithologies, including interbedded sandstone, siltstone, mudstone and coal (Carvell et al., 2014), granite (*sensu lato*; Mitra, 1979 and Bertini et al., 1985) and banded gneiss (Beacom et al., 1999). Koestler and Ehrmann (1991) and Miller et al. (2007) have described polymodal fault patterns in chalk, limestone and dolostone. Most authors infer that the faults making up the pattern were contemporaneous based on mutual offsets and cross-cutting relationships observed in outcrops or in map pattern.

In summary, polymodal fault patterns with orthorhombic symmetry have been reported from igneous, metamorphic and sedimentary rocks, suggesting there is no special lithological control on their formation. Polymodal patterns have been formed in divergent, transcurrent and convergent settings. Polymodal fault patterns occur on a wide range of length scales, from single outcrops (10^{-2}–10^{1} m) to regional scale (10^{3}–10^{5} m). To date, few authors have tabulated or quantified the critical evidence for simultaneous activity on the multiple fault sets making up polymodal fault arrays. However, Healy et al. (2006b) used a matrix of observed cross-cutting relationships to document the contemporaneity of the fault sets in the polymodal pattern at Gruinard Bay, Scotland, based on younging tables (Angelier, 1991; Potts and Reddy, 1999).

3. Laboratory examples

3.1. Analogue materials

Oertel (1965) conducted a series of elegant experiments using blocks of kaolinite + water clay paste deformed under conditions of truly triaxial strain. He found that four sets of faults with orthorhombic symmetry developed in the clay for tests involving either elongation or shortening. Using piezometers embedded in the clay, he established that the state of stress was nearly homogeneous and coaxial with the strain. His clay material exhibited strain-hardening behaviour. Oertel (1965) concluded that the orientations of the fault planes and the slip directions on them did not agree with the Coulomb theory of fracture. He proposed a model based on the

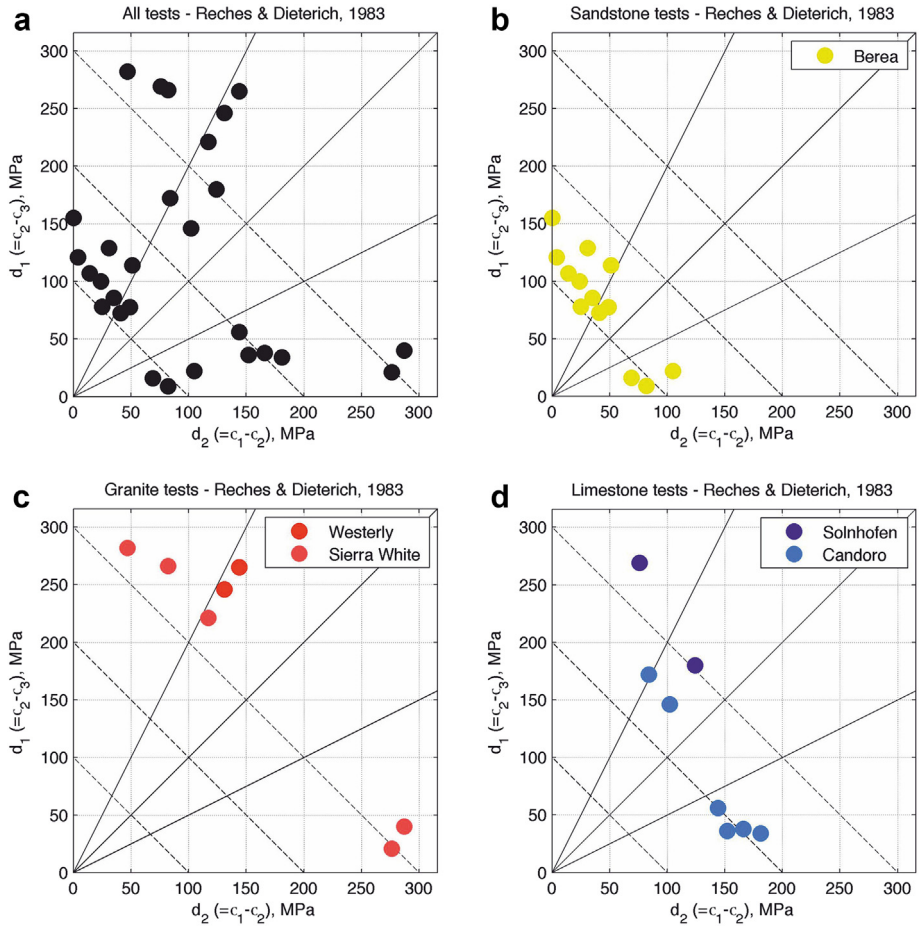

Fig. 4. Experimental data from Reches and Dieterich (1983) on a Lisle (1979) stress plot. This plot shows a range of geologically viable and more likely natural stress states. The vast majority of previous conventional 'triaxial' rock deformation experiments would plot along the x-axis, where $d_1 = (\sigma_2 - \sigma_3) = 0$ (i.e. $\sigma_2 = \sigma_3 =$ confining pressure). Data are taken from the peak stresses tabulated in Reches and Dieterich (1983, their Table 1) for truly triaxial stress test on a range of different rock types. Plot a) shows the peak stresses for all rock types ($n = 28$), b) is for tests on sandstone ($n = 13$), c) tests on granite ($n = 7$), d) tests on limestone ($n = 8$).

assumptions that deformation occurred solely by slip on the faults, that the faults interacted with one another and that the bulk deformation maximised the rate of work done for a given stress.

Other workers have used clay models to explore the boundary conditions of oblique rifting – i.e. extension perpendicular to the rift trend accompanied by shear parallel to the trend. Withjack and Jamison (1986) produced patterns of normal and strike-slip faults in their clay cakes, classified as a function of the acute angle (α) between the rift trend and the relative displacement direction between the opposing sides of the rift. Polymodal patterns of faults were produced for $30° < \alpha < 90°$, although the inherent vorticity of the applied strain field resulted in a marked asymmetry of fault orientations. This is apparent in the rose diagrams of fault strike normalised by fault trace length (Withjack and Jamison, 1986; their Fig. 7). Smith and Durney (1992) corroborated these findings using a finer subdivision of divergence angles (α).

3.1.1. Rock deformation experiments

Reches and Dieterich (1983) subjected 31 small cubes (2.2 cm on a side) of granite, sandstone and limestone to truly triaxial stresses using an apparatus with three pairs of mutually independent, perpendicular presses. Most of the samples displayed three or four sets of shear fractures with orthorhombic symmetry. However, samples constrained to plane strain deformation displayed conjugate (bimodal) faults. For the orthorhombic fault patterns, poles to faults lie within a 26° small circle centred on the direction of ε_1 (greatest extensional strain) and σ_3 (least compressive stress) (Reches and Dieterich, 1983; their Fig. 5). Reches and Dieterich (1983) observed a strong effect of lithology on the polymodal fault patterns. The largest angles between the four sets of faults were found for the sandstones (i.e. greater dispersion of poles to faults on the equal angle nets), followed by the limestones and then the granites with the smallest inter-fault angles. This is empirical evidence of a strong material effect in the patterns of polymodal faulting under truly triaxial stress.

Fig. 4 shows the data from Reches and Dieterich (1983) plotted on a Lisle stress diagram (Lisle, 1979), which allows us to appreciate the truly triaxial 'stress space' of the experiments. The origin of this plot represents hydrostatic stress (or pressure), and the x-axis (d_2) is the locus of all axial compression tests. The vast bulk of conventional 'triaxial' deformation experiments would plot along this axis. In these tests, $\sigma_1 > \sigma_2 = \sigma_3$ and the load is axisymmetric with respect to the cylindrical core plug sample geometry. Diagonal lines from the origin show the R ratio ($=d_1/d_2$), and diagonal lines with a slope of -1 (dashed in Fig. 3) show different values of differential stress ($=\sigma_1 - \sigma_3$). The experiments on sandstone, granite and limestone cover a wide span of triaxial stress space. These experiments represent the best laboratory evidence to date of polymodal fracture patterns comprising three or four sets of faults forming under truly triaxial stress. Moreover, these experiments also

confirm that under plane strain, only two sets of faults form, consistent with the restrictions of the Mohr-Coulomb failure criterion.

Further experiments using a similar overall design of apparatus have recently been conducted by a group at the University of Toronto (Ghaffari et al., 2014; Nasseri et al., 2014). Their apparatus incorporates transducers into the loading platens for recording acoustic emissions (AE), allowing them to track the nucleation and growth of the shear failure planes during the loading. Experiments on cubic samples of sandstone (8 cm on a side) produced polymodal fault systems 'with varying degrees of obliquity to the directions of principal stresses' clearly visible on the sample faces and in the clouds of located AE hypocentres. These authors also note that tensile-mode microcracks dominated the pre-peak deformation of their samples, and these microcracks were oriented parallel to the σ_1–σ_2 principal plane, i.e. normal to σ_3.

In summary, experiments with analogue materials such as clay-water mixtures and with rock specimens of different lithologies have all shown that polymodal fault patterns form in response to the controlled imposition of truly triaxial strain and/or stress. These fault patterns display orthorhombic symmetry, comprising clusters of three or, more commonly, four sets of shear failure planes. Fault planes in these sets are observed to form and slip simultaneously, and they are oblique to all three principal stresses (or strains). These fault patterns are, therefore, fundamentally inconsistent with the predictions of the Mohr-Coulomb failure criterion.

4. Kinematic, or strain-based models

Based on the results of his clay cake experiments, Oertel (1965) developed a kinematic model for the orientations of the four fault sets in response to triaxial strain. His model is based on several assumptions, in turn derived from his observations of the fault patterns that evolved in the experiments. His assumptions included the following: deformation is solely by slip along the fault planes, moving faults interfere with the mobility of other faults, friction and viscous drag offer resistance to slip along the fault planes, and the deformation maximises the rate of work for the given stress. Oertel (1965) presented a hypothesis of interfering slip planes, based on summing the strain rates on each of four families of fault planes into a bulk orthorhombic strain rate.

Reches (1978, 1983) developed a similar model to explain polymodal fault patterns observed in outcrops and in truly triaxial rock deformation experiments. His assumptions were that: the rock originally contains many surfaces of discontinuity with random orientations, the deformation is solely by slip along fault planes, the favoured fault sets minimise the dissipation of work under a given strain, and that resistance to slip along the faults obeys Coulomb's law i.e. shear stress depends on normal stress. Reches (1978, 1983) emphasised that his model is a slip criterion, not a failure criterion: the fault planes are assumed to already exist throughout the rock, and therefore their nucleation is not explained by the equations he presents. Reches (1983) presented expressions for the orientations of the four fault sets and their slip directions in terms of the strain ratio k ($k = \varepsilon_2/\varepsilon_3$) and the angle of friction ϕ.

Krantz (1988, 1989) developed the odd-axis model based, in part, on the slip model of Reches (1978, 1983). Assuming that deformation is achieved solely by slip along the faults, is irrotational, is constant volume, and is equally distributed among the fault sets, Krantz (1988, 1989) recognised that one of the principal strains will have a different sign from the other two: this is the odd-axis. Using the geometric relationships inherent in the slip model, Krantz (1988, 1989) showed that the odd-axis lies at the common intersection of planes containing the poles to the fault planes and their slip vectors (Krantz, 1988; his Fig. 4). The angle between these planes is related to the ratio of the principal strains. Application of the odd-axis method to the Chimney Rock fault array in Utah (USA) shows that this angle is 48°, predicting a ratio of $\varepsilon_2/\varepsilon_1$ of 0.2 and $\varepsilon_2/\varepsilon_3$ of 0.16, providing that the ratio of fault slip to spacing is small, as observed at Chimney rock (Krantz, 1988). The odd-axis model is therefore more of a method for analysing polymodal, orthorhombic fault patterns, rather than a criterion for their formation *per se*.

5. Mechanical, or stress-based models

In addition to his kinematic slip criterion, Reches also presented a faulting criterion for truly triaxial stress (Reches, 1983; his equation (28)):

$$J_2 = aJ_1^b$$

where J_1 is the first stress invariant ($\sigma_1 + \sigma_2 + \sigma_3$) and J_2 is the second stress invariant ($\sigma_1\sigma_2 + \sigma_2\sigma_3 + \sigma_3\sigma_1$), and a and b are empirical coefficients determined from curve fitting of the experimental data. With correlation coefficients from this curve fitting exceeding 0.96, Reches found that a varies from 0.15 to 0.23 and b varies from 2.14 to 2.35, depending on the lithology used in the experiments described in Reches and Dieterich (1983). However, Reches (1983) could find no relationship between this faulting criterion and his slip criterion, in order to link the truly triaxial stresses to the predicted orientations of the fault planes.

Healy et al. (2006a, 2006b) developed a model for polymodal fault nucleation based on the 3D interactions of tensile microcracks. Derived from a similar 2D model of Reches and Lockner (1994) and motivated by the earlier 3D analyses of Murrell and Digby (1970a, 1970b), the 3D model assumes that shear failure planes (faults) form from the coalescence of tensile microcracks (e.g. Lockner et al., 1991). Healy et al. (2006a, 2006b) modelled the elastic stress field in the volume around an oblate ellipsoidal void, considered as a proxy for a tensile microcrack oriented parallel to the σ_1–σ_2 principal plane (normal to σ_3) in a deforming rock (see Fig. 5a and b).

Using the established formalism of Eshelby (1957, 1959), Healy et al. (2006a, 2006b) show that the locus for maximum tensile interaction around each void (or microcrack) is a surface oblique to all three principal stresses. The inference is that the elastic interactions and the eventual coalescence of a population of tensile microcracks will occur along these oblique surfaces. For an isotropic elastic material, these surfaces of maximum tensile interaction display an acute half-angle of 26° with respect to σ_1 and σ_2. Alternatively, poles to faults formed along these surfaces would lie along or within a small circle of 26° centred on σ_3, the least compressive principal stress (e.g. Fig. 5c).

Blenkinsop (2008) looked at the geometrical relationships between faults, extension fractures (including veins) and stress. According to Mohr-Coulomb theory, faults and extension fractures formed in a single deformation event should strike parallel to each other, their line of intersection should lie parallel to the inferred direction of σ_2 and normal to the slip direction on the fault. However, for reactivated or polymodal faults, these restrictions no longer hold. Blenkinsop derived expressions for the general relationship between shear planes, extension fractures and principal stresses. An angle θ exists between the fault-fracture intersection and the direction of maximum resolved shear stress, and can vary from 0 to 90°. Andersonian faults, formed according to the Mohr-Coulomb criterion should have $\theta = 90°$ (see Fig. 6). Blenkinsop tabulated the findings from three field studies, where the contemporaneity of shear fractures and extension fractures could reliably be established, and found that θ varied from 52 to 66° (Blenkinsop, 2008; his Table 2). This is inconsistent with the Mohr-Coulomb failure criterion.

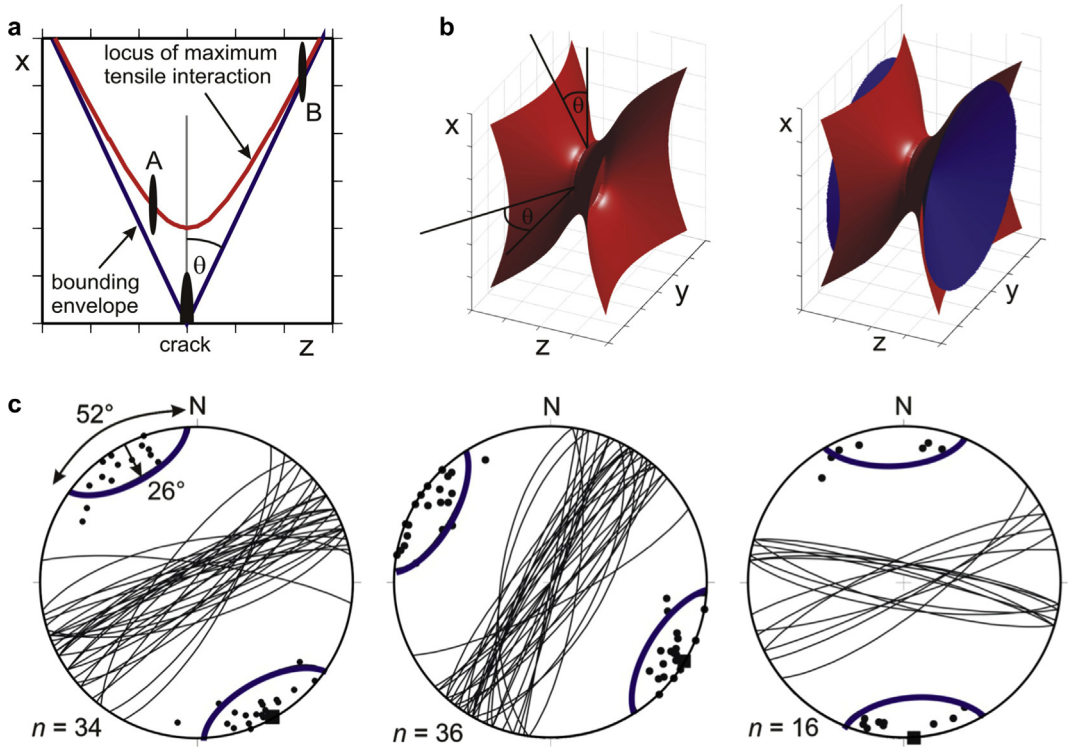

Fig. 5. Details of the model proposed by Healy et al. (2006a, 2006b), together with orientation data from deformation bands at Gruinard Bay, Scotland (UK). The 2D plot in a) shows the locus of maximum tensile interaction for the half-space above a tensile elliptical crack embedded in an isotropic elastic medium. This is the core of the model proposed by Reches and Lockner (1994). The 3D plots in b) show the locus of maximum tensile interaction as hyperbolic surfaces symmetrically disposed about the ellipsoidal tensile crack (hidden at the centre of the plots). For tensile microcracks oriented normal to σ_3 and lying in the σ_1–σ_2 principal plane, this model predicts that shear failure surfaces will form from the interaction and coalescence of cracks along these surfaces. For isotropic elastic materials, the surfaces make angles of 26° with σ_1 (X in this reference frame) and σ_2 (Y in this reference frame). c) Equal angle nets of data collected from deformation bands in contiguous outcrops of Triassic sandstone at Gruinard Bay, Scotland. Note that the orientations of poles to deformation bands are distributed within small circles of about 26°, consistent with the experiments of Reches and Dieterich (1983) and the angles between tensile and shear fractures measured by Blenkinsop (2008).

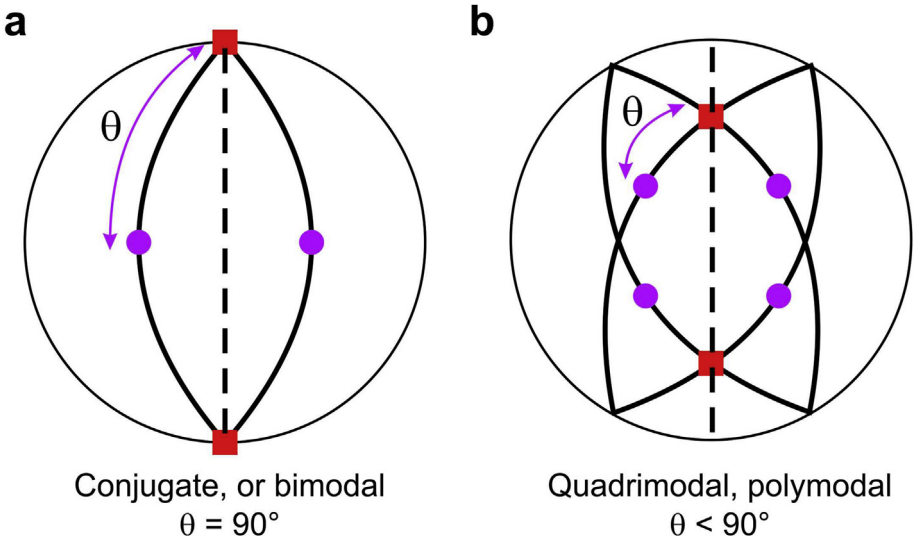

Fig. 6. Equal angle nets illustrating the key point from Blenkinsop (2008). Coeval tensile (dashed lines) and shear fractures or faults (solid lines) are shown for the conjugate (bimodal) case in a) and the quadrimodal case in b). Slip vectors are shown by mauve dots on the shear planes, and intersections of tensile and shear fractures are shown by red squares. θ denotes the angle – measured in the shear plane – between the slip vector and the intersection of the tensile and shear fractures. For conjugate (bimodal) faults $\theta = 90°$, whereas for quadrimodal faults $\theta < 90°$. Field observations listed in Blenkinsop (2008) show that θ lies between 52° and 66°.

Ghaffari et al. (2014) proposed a new component to the nucleation of polymodal faults, based on their analysis of acoustic emission waveforms recorded during rock deformation experiments under truly triaxial stress. After confirming that faults form in orthorhombic patterns, these authors used the rise-times of acoustic events to infer that microscale 'anticracking' was occurring in the samples. Ghaffari et al. (2014) report volume reductions oriented preferentially parallel to σ_3 which they refer to as

compactant anticracks on the basis of AE waveforms. Dilatant microcracks produced distinctly longer rise-times than compactant microanticracks in their samples. The anticracks are described as being parallel to σ_3, but no orientation statistics have yet been presented. If confirmed, this finding offers a connection to rupture models for deep earthquakes involving anticracks from mineral phase changes (Green et al., 1990; Healy et al., 2006c).

The Mohr-Coulomb failure criterion does not include a term for σ_2, and cannot therefore explain fault planes oriented oblique to all three principal stresses or the dependence of rock strength on σ_2. Other failure criteria, such as Hoek-Brown, Drucker-Prager, Lade (and Lade-Duncan) and Mogi have been published and are more widely used in disciplines such as engineering (see Haimson, 2006 and Ulusay and Hudson, 2012 for recent reviews; Singh et al., 2011 for a modified Mohr-Coulomb expression). However, it is important to note two details of these truly triaxial failure criteria: none predicts the orientations of the failure planes, and some have been 'adjusted' to *explicitly preclude* any effect of σ_2 on the orientations of failure planes e.g. the Mogi criterion (see Al-Ajmi and Zimmerman, 2005). The applicability to polymodal faulting of the various plastic yield criteria proposed by Tresca, von Mises and Hencky (see Jaeger et al., 2009 for a modern review) – which incorporate the intermediate principal stress σ_2 through their use of stress invariants – were summarised by Oertel (1965) as follows: 'they … do not make any statements, not even implicitly, about the attitudes of planes of failure. Consequently they are inappropriate for a solution of the problem at hand.'

6. Discussion

6.1. Recognition of polymodal fault patterns from outcrops and maps

From the above it is clear that the orientation distribution of faults or shear failure planes formed under a homogeneous triaxial stress regime is a key piece of data. However, the measurement, analysis and presentation of these data require care. The following points arise from the previously published accounts:

- Although many natural fault surfaces are in detail curviplanar, outcrop measurements are commonly taken by 'planar orientation averaging' – e.g. using a notebook or map-board to approximate the tangent to a curviplanar surface at a given measurement point. There is evidently a critical scale beyond which 'planar orientation averaging' should not be done. Therefore, it is possible that many field examples of polymodal fault patterns are not recognized due to the way that planar data are collected (e.g. inappropriate application of 'planar orientation averaging', or inherent subjectivity of the field geologist). But this does beg the question – when should 'planar orientation averaging' be applied in the field, and to what extent? Some fault surfaces are truly continuously curved, whereas some are made of planar segments. A full discussion of this issue is beyond the scope of this paper, but we believe this topic deserves further analysis.
- The most robust data (for any aspect of a fault pattern) will come from large areas of contiguous outcrop where stress can be assumed or reasonably inferred to be homogeneous. Data from disparate, disconnected outcrops may suffer from unknown stress heterogeneities or block rotations, which render the orientations less useful.
- There is a need to establish orientation distributions through measured fault plane data, plotted on equal angle or equal area nets. Photographs of *apparently* conjugate fault traces on 2D sections alone are *insufficient* to establish the conjugate (bimodal) nature of fault patterns, although this is very commonly presented in the literature (e.g. Cilona et al., 2012). We advise the use of the term 'apparently conjugate', unless an equal angle net of measured orientations is supplied with the photograph or sketch.
- There is a need to establish clear evidence of central tendency for allegedly bimodal/conjugate or quadrimodal fault patterns. If this is lacking, then the pattern can reasonably and simply described as polymodal, an objective term describing the orientation data distributed over a limited range of strikes and dips. Wider and more rigorous use of spherical statistics is encouraged (e.g. Fisher et al., 1987; Mardia and Jupp, 2009).
- Detailed documentation of the evidence for the simultaneous activity of all sets in a polymodal fault array is as essential as plotting carefully-made orientation measurements on equal angle or equal area nets. Wider use of the matrix of cross-cutting relationships (e.g. Healy et al., 2006b; based on Potts and Reddy, 1999) is strongly recommended.

6.2. Issues with the results of rock deformation experiments

Some of the first systematic rock deformation experiments under truly triaxial stresses were conducted by Mogi (e.g. 1967, 1971a, 1971b). Mogi built an apparatus that provided biaxial compressive stresses on rectangular prism shaped specimens through two sets of pistons for σ_1 and σ_2, with confining pressure ($=\sigma_3$) acting on the front face. From experiments on a granite and two carbonate rocks, Mogi determined that increasing σ_2 causes the angle between the shear failure plane and σ_1 to decrease (Mogi, 1967; his Table 2), and that shear fractures formed 'very nearly parallel to σ_2', without providing any measured angles for this assertion. The specimen shape in these tests may have had an effect on the shear fracture orientation: samples were 1 cm thick (in the σ_3 direction), 1.6 cm wide (σ_2 direction) and 3.7 cm high (σ_1 direction). The shear fracture was therefore constrained to occur within a very narrow (1 cm) tablet of rock, and would be constrained to form 'nearly parallel to σ_2'. In subsequent experiments on samples of granite, volcanic rocks, and other carbonate rocks, the specimen dimensions were changed to 1.5 cm square by 3 cm high, and similar results were found: the angle between σ_1 and the shear failure plane decreased with an increase in σ_2 and shear failure occurred on planes 'parallel to σ_2' (Mogi, 1971a, 1971b).

These results *could* be problematic for a general theory of polymodal failure, but any quantitative, systematic analysis of the experimental data is impossible because the angles of the faults with σ_2 – however small or variable – are not tabulated in these papers. Moreover, the claims of some authors that shear fractures produced on the Mogi-type apparatus are 'parallel to σ_2' are substantially undermined by clear evidence to the contrary displayed in their own photographs of faulted samples e.g. Chang and Haimson (2000, their Fig. 16b and c; or 2005, their Fig. 15c).

For the vast majority of published laboratory rock deformation data based on conventional 'triaxial' (axisymmetric) loading of cylindrical samples, it is impossible to say whether the shear fractures produced are bimodal (conjugate) or polymodal when σ_2 is constrained to be equal to σ_3 (Fig. 7). The imposition of the radial confining pressure ($P_c = \sigma_2 = \sigma_3$) means that the reference frame cannot by definition be used for orientation measurements related to the effect of σ_2.

6.3. Boundary conditions and simplifying assumptions

As noted above, conventional triaxial laboratory tests based on

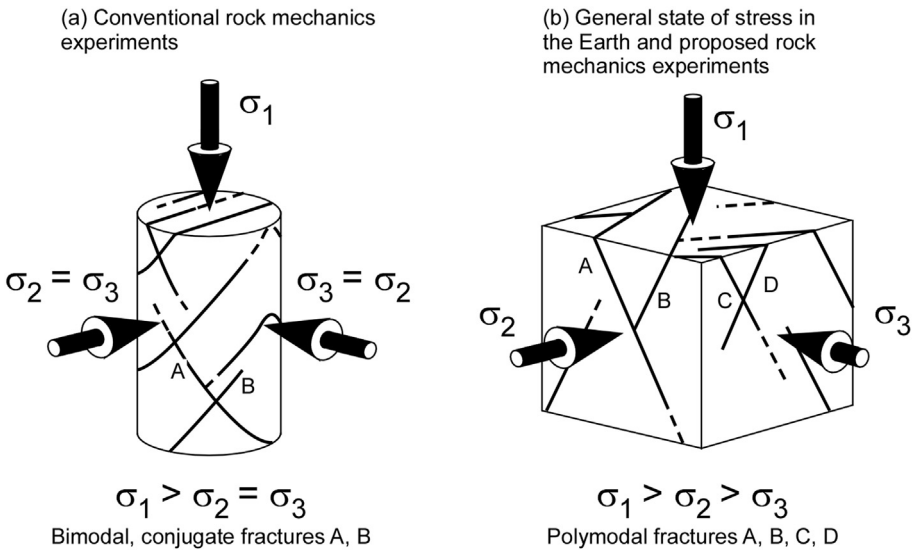

Fig. 7. Schematic diagrams highlighting the difference between conventional 'triaxial' stress states used in rock deformation experiments, and the truly triaxial stress state considered more likely in the Earth. Axisymmetric stress states in experiments provide *no information* on the relative orientation of fault planes to the intermediate principal stress.

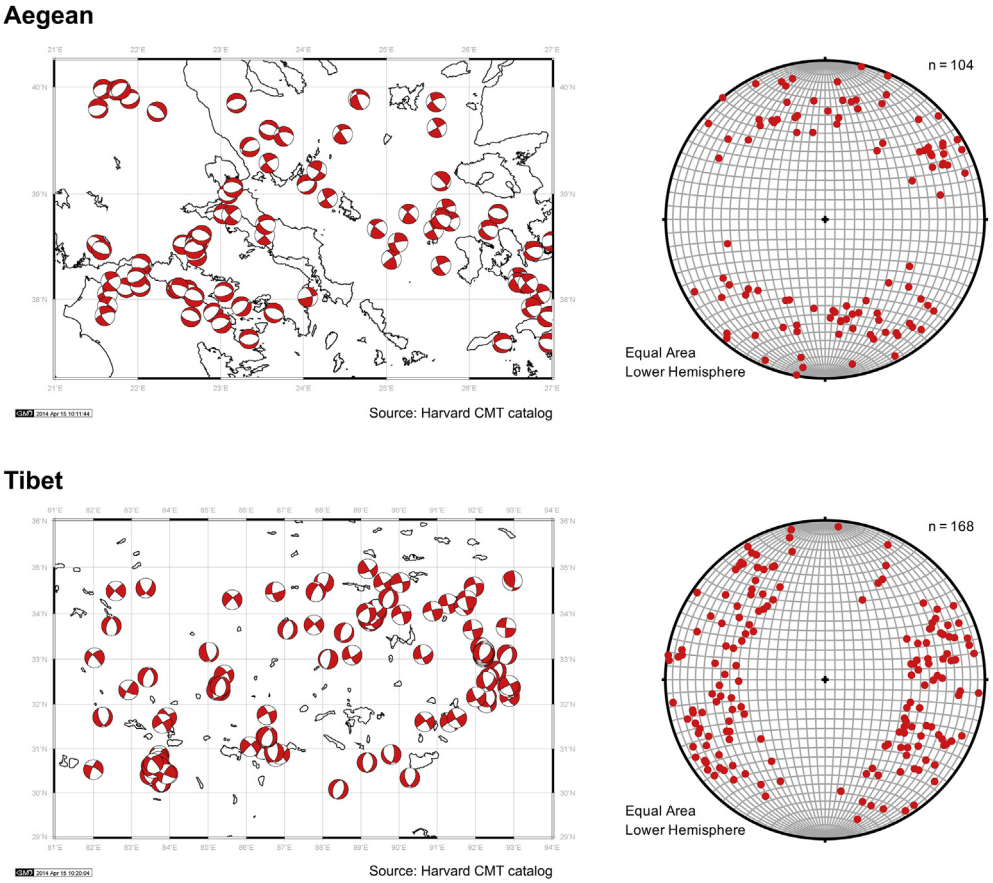

Fig. 8. Maps showing focal plane solutions from Aegean and Tibet, with equal angle nets of poles to steeper planes. Using data from the Harvard CMT catalogue (Ekström et al., 2012), these maps show two areas of active extension. Andersonian mechanics would predict a simple pattern of sub-parallel normal faults and plane strain. Note the range in nodal plane orientations, especially their strikes. The stereographic projections show only the poles to the steeper planes, i.e. ignoring the possible role of low angle normal faults, but the signal is clear: the fault planes are not *clustered* about two conjugate directions, they are evenly distributed over a significant arc of strike i.e. a *polymodal* fault pattern, in both cases. Maps produced using the Generic Mapping Tools (GMT, Wessel et al., 2013).

axisymmetric stress fields cannot be used to discriminate between bimodal and polymodal fault patterns. Geological strain and stress patterns will, in general, be 3D and truly triaxial. That geological stresses are triaxial is established in Lisle et al.'s (2006) review of faulting, which shows that the modal value of the stress ratio $(=(\sigma_2-\sigma_3)/(\sigma_1-\sigma_3))$ is 0.39. Further evidence in support of the generally triaxial nature of deformation comes from seismicity in regions of active deformation. Focal plane solutions from the

Harvard CMT catalogue (Ekström et al., 2012) for two regions of active extension are shown in Fig. 8. Both the Aegean and Tibetan regions are currently dominated by extensional strain driven by wider plate movements. The earthquake focal mechanisms – albeit restricted to a geologically trivial time window of 40 years or so – reveal a complex pattern of strain accumulation through normal and strike-slip faulting. Equal angle nets of poles to (steep) faults show no distinct bimodal clusters. The orientation data are distributed over finite arcs of both strike and dip. Objectively, these are polymodal fault patterns and they represent snapshots of the active fault systems that have developed to accumulate finite strain in these extending regions of the crust.

Reches (1983) makes the crucial point that faulting is usually analysed under one of two different approaches: either with a yield criterion *based on a postulate or empirical data* (e.g. Mohr-Coulomb, von Mises, Tresca etc.), or alternatively using a *prescribed mechanism of yielding* which is then related to yield stresses (e.g. Griffith, Oertel, Reches). Yield – or failure – criteria of the first type suffer from various issues. For example, Coulomb suggested that the key control for frictional sliding on a fault is the ratio of shear stress to normal stress acting on the fault plane, what we now call the slip tendency T_s ($T_s = \tau/\sigma_n$; Morris et al., 1996). Mohr extended this to include the concept of this slip tendency ratio exceeding a limit, i.e. the frictional strength. While this postulate has matched the data from the early experiments, dominated by inclined sliding blocks and conventional triaxial laboratory tests, it carries an inherent but severe limitation: the symmetry of slip tendency for truly triaxial stress fields is bilateral, not orthorhombic. Specifically, for general triaxial stress states where $\sigma_1 > \sigma_2 > \sigma_3$, there are only two slip tendency maxima, symmetrically disposed along the σ_1–σ_3 principal plane. The fundamental limitation of the Mohr-Coulomb theory then becomes readily apparent: poles to faults are predicted to lie within, or statistically close to, either of these two maxima. Observations of polymodal fault patterns from outcrops and experiments cannot be explained by Mohr-Coulomb theory due to this fundamental argument based on the inherent symmetry. The Mohr-Coulomb theory can however predict polymodal fault patterns when the stress state is axisymmetric – i.e. either $\sigma_1 = \sigma_2$ or $\sigma_2 = \sigma_3$, in which case the zones of maximum slip tendency now form circular arcs around either σ_3 or σ_1, respectively (see Fig. 9).

None of the published failure criteria acknowledge an important observation from the work of Oertel (1965): that polymodal fault patterns involve *populations* of many faults, nucleating, growing, slipping and presumably 'dying' during the deformation. Oertel went on to consider how these interactions could be explicitly incorporated into a kinematic model of orthorhombic strain, but this approach has not been developed since. Failure criteria linking principal stresses and rock properties to strength, and ideally, failure plane orientation, may need to include the dynamic effects of multiple fault sets in the failure process.

Failure criteria independent of the geometric constraints of

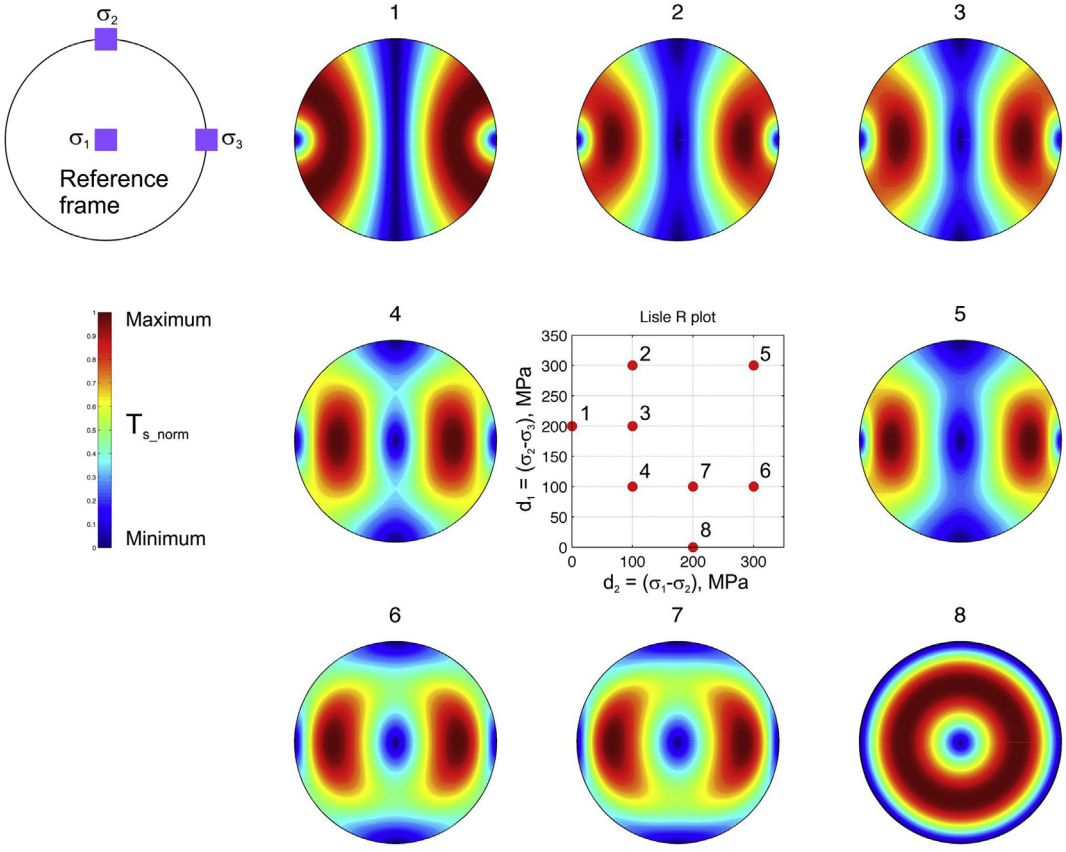

Fig. 9. Equal area nets showing the directional variation in slip tendency T_s ($=\tau/\sigma_n$) for different triaxial stress regimes. Any point on the net represents a pole to a potential fault plane, and the colour denotes the normalised slip tendency T_s/T_{max}. Red colours denote high values (likely to slip), and blue colours denote low values (unlikely to slip). Examples from eight stress regimes are shown with σ_1 vertical, σ_2 horizontal trending north-south, and σ_3 horizontal trending east-west. Slip tendency is the central failure criterion at the heart of the Mohr-Coulomb model for shear failure. Note the prevalence of bilateral symmetry in the patterns of slip tendency (examples 2–7), *except* for axisymmetric stress fields where either $\sigma_1 = \sigma_2$ or $\sigma_2 = \sigma_3$ (examples 1 and 8). The Mohr-Coulomb model predicts that for truly triaxial stress fields ($\sigma_1 > \sigma_2 > \sigma_3$, examples 2–7), faults will tend to form in one of two conjugate directions, with poles clustering in either of the two red maxima of slip tendency. This is at odds with the outcrop and laboratory evidence for polymodal, non-conjugate, fault patterns under these conditions of truly triaxial stress.

Mohr-Coulomb theory include work minimisation and limit analysis. Work minimisation can find the fault surfaces that minimize or maximize various terms within the work budget including internal work, (e.g. Cooke and Madden, 2014, and references therein). For example, Reches (1983) shows that the four fault sets to form under truly triaxial loading can minimize both the dissipation of the volume or internal work, which is the stress times strain, and the applied differential stress ($\sigma_1 - \sigma_3$). The minimisation of the applied differential stress parallels the approach of minimizing external work through finding the fault network that requires the least applied stress to accommodate the applied strain.

The minimisation of external work on a system is similar in approach to the upper bound of limit analysis, which finds the maximum external work that the system can sustain before failure. This approach predicts the arrangement of faults that produces the lowest maximum external work (e.g. Maillot and Leroy, 2006). Limit analysis also incorporates a lower bound via the maximum strength theorem, which finds the largest stress state that is within the failure limit (e.g. Pons and Leroy, 2012). Elastoplasticity provides a convenient framework to unite the upper and lower bounds of limit analysis to find a true solution, such as implemented within critical state soil mechanics (e.g. Chen, 1975). Three-dimensional implementations of limit analysis and work minimisation may provide crucial insights into polymodal fault system development.

6.4. Rheology; rock properties; anisotropy

There is a widely reported difference in the brittle behaviour of porous granular rocks and tight crystalline rocks (e.g. Renner and Rummel, 1996; Zhu and Wong, 1997; Fossen et al., 2007). Reches and Dieterich (1983) noted significant differences in the measured polymodal fault patterns in rock deformation experiments on sandstone, limestone and granite. Berea Sandstone samples, with the highest initial porosity, displayed the widest range in orientation distribution and the best fit to the slip model predictions, whereas Candoro and Solnhofen Limestone samples had narrower ranges of orientations. Westerly and Sierra White Granite patterns provided the worst fit to the slip model predictions and the narrowest range of polymodal fault orientations. This lithological influence on the polymodal fault orientation distribution remains unexplained, but is a key component in the quest to formulate a generally applicable, truly triaxial, failure criterion.

Polymodal faulting – as for any kind of localisation behaviour – should be analysed in a framework of critical state soil mechanics (e.g. Aydin et al., 2006). The underlying elastoplasticity theory predicts localisation when the determinant of the acoustic elastoplastic tensor – a function of the orientation of a possible failure plane – is zero. Such a prediction would be testable if we had detailed datasets for the evolution of the elastoplastic constitutive tensor under truly triaxial conditions.

Polymodal faulting has not yet been reported in highly anisotropic rocks such as gas shales. Predicting fracture patterns in these tight rocks, especially with respect to fracture connectivity, is critical for the development of approaches to enhancing permeability, e.g. through hydraulic fracturing. Scope exists to explore and quantify how a truly triaxial stress tensor interacts with a strong fabric tensor during brittle deformation of these rocks. Experimental work on schists has shown that strong fabrics can result in polymodal fault planes oblique to all principal stresses, even using a Mogi-type apparatus (Kwaśniewski, 2012).

7. Suggestion for a kinematic approach to polymodal faulting

We are left with the apparent paradox of a truly triaxial stress tensor ($\sigma_1 > \sigma_2 > \sigma_3$) with orthorhombic symmetry, producing truly triaxial strains ($\varepsilon_1 > \varepsilon_2 > \varepsilon_3$) on polymodal faults with orthorhombic symmetry, and yet the dominant framework for understanding this deformation – the Mohr-Coulomb failure criterion – displays bilateral symmetry. To address this fundamental physical issue, we can question whether a stress-based failure criterion is the correct or best paradigm for understanding brittle failure in rocks. There is a long-standing debate in structural geology about the relative primacy of stress or strain (or displacement) as the key driver of deformation. Several authors have promoted a kinematic perspective, asserting that displacement and strain are the primary drivers of tectonic deformation, and that stresses are more local and simply accommodate the strain (Tikoff and Wojtal, 1999; Watterson, 1999). This viewpoint is made more attractive by the simple fact that both strain and displacement are measurable quantities, in the field and the laboratory.

Watterson (1999) made a compelling argument for faults and shear zones forming parallel to surfaces of no finite longitudinal strain (hereafter, *nfls*). For any observed 3D strain, there are surfaces across which the normal, or longitudinal, strain is zero (Ramsay, 1967). For a plane strain, these surfaces are circular planes and sections of the strain ellipsoid. For all other non-plane strains, the surfaces are more complex and not planar. We can extend the analysis of Watterson, who assumed plane strain as the "the bulk strain most commonly associated with faulting" (Watterson, 1999), into more general 3D strains such as oblate flattening.

Fig. 10 shows schematic block diagrams of faults and the respective Mohr circles for strain for two different plane strains: one with no volume change ($\Delta V = 0$, Fig. 10a) and one with positive dilatation ($\Delta V > 0$, Fig. 10b). For plane strain and no volume change, faults (or shear zones) forming parallel to surfaces of *nfls* are predicted to form at 45° to the maximum shortening (ε_z), and parallel to the intermediate strain (ε_y, = 0 in this case). This angular relationship is derived from the Mohr circle for strain. Point A in the Mohr plot marks the intersection of the strain circle for the *xz* plane with the *y*-axis, where the normal strain $\varepsilon_n = 0$. Therefore, the line from the origin to A marks the locus of all lines of *nfls*. This line gives the angle $2 * \alpha_{xz} = 90°$, and therefore $\alpha_{xz} = 45°$. Watterson showed that with a positive volume change (Fig. 10b), α_{xz} can increase above 45°, and approach the commonly observed 60°–70° dip angle of normal faults, for reasonable volume changes (Watterson, 1999). For plane strains, a simple kinematic model of faults forming parallel to surfaces of *nfls* predicts bimodal (conjugate) faults dipping at $\pm\alpha_{xz}$.

The existence of polymodal faults in the field and the laboratory leads us to suggest an extension to Watterson's (1999) analysis. Fig. 11 shows schematic block diagrams and corresponding Mohr strain circles for oblate, non-plane strain deformation. In Fig. 11a, we illustrate the case of uniaxial shortening with $\varepsilon_x = \varepsilon_y$, corresponding to the vast majority of laboratory rock deformation tests under axisymmetric load with a constant confining pressure on a cylindrical sample. For the relative magnitudes of strains shown, a fault forming parallel to the surface of *nfls* will be oriented at a dip angle > 45°, but note that it could form in any orientation with respect to the *x*, *y* reference axes in a conical locus about ε_z. In the case of a general oblate strain with $\varepsilon_x > \varepsilon_y > \varepsilon_z$, faults forming parallel to surfaces of *nfls* will be oriented in one of four possible orientations (i.e. 2 sets of conjugates) with respect to the axis of shortening. The fault orientations are now defined by the angles α_{xz} and α_{yz} in the XZ and YX principal planes, respectively. These angles are trace angles, or angles of pitch, on those principal surfaces: they are angles of apparent dip, and the *true* orientations of the fault planes are predicted to be oblique to all three principal strains (Fig. 11b). Angles α_{xz} and α_{yz} are given by:

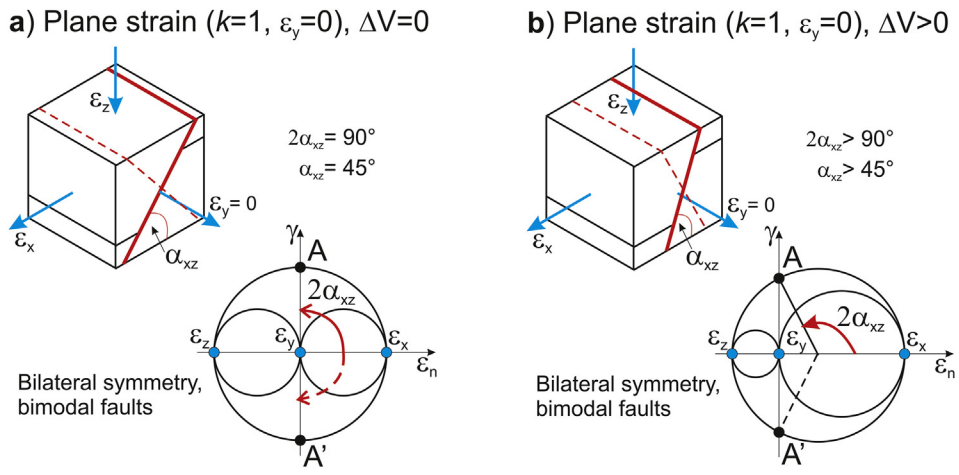

Fig. 10. Schematic block diagrams of strained rock volumes and corresponding Mohr diagrams depicting the strain state. a) For an arbitrary plane strain ($\varepsilon_y = 0$) and no volume change, faults forming parallel to surfaces of no finite longitudinal strain (*nfls*) are predicted to occur at ±45° to the shortening direction, and their intersection will run parallel to ε_y. b) For a plane strain ($\varepsilon_y = 0$) with a positive dilatation ($\Delta V > 0$), the dip angle of the faults is predicted to steepen (>45°), although the symmetry remains the same as the case for no volume change.

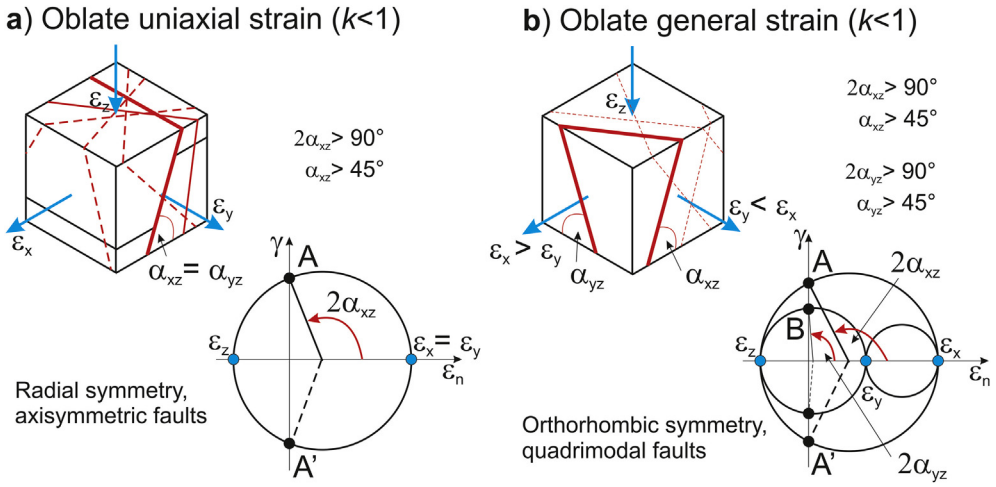

Fig. 11. Schematic block diagrams of strained rock volumes and corresponding Mohr diagrams depicting the strain state. a) For an oblate uniaxial strain with $\varepsilon_x = \varepsilon_y$, fault forming parallel to surfaces of *nfls* will form at angle $\alpha_{xz} = \alpha_{yz} > 45°$ to the shortening axis, and with radial symmetry about this axis. b) For a general oblate strain with $\varepsilon_x > \varepsilon_y$, the angles α_{xz} and α_{yz} are no longer equal. These angles represent trace angles on the principal planes of bulk strain (XZ and YZ), and the faults that form parallel to surfaces of *nfls* will, in general, be obliquely inclined to all three principal strain axes. The orientations of the faults depends on the magnitudes of the principal strains (ε_x, ε_y, ε_z) and the degree of dilatation (ΔV).

$$\alpha_{xz} = \frac{\pi}{2} - \frac{\cos^{-1}\left(\frac{(\varepsilon_x+\varepsilon_z)}{(\varepsilon_x-\varepsilon_z)}\right)}{2}$$

$$\alpha_{yz} = \frac{\pi}{2} - \frac{\cos^{-1}\left(\frac{(\varepsilon_y+\varepsilon_z)}{(\varepsilon_y-\varepsilon_z)}\right)}{2}$$

From the angles α_{xz} and α_{yz}, and the trigonometry of apparent dip (e.g. Ragan, 2009), we can determine the strike and dip of the faults in a geographical reference frame. Alternatively, expressions for the principal strains can be derived from measurements of the fault apparent dips (α_{xz} and α_{yz}) and the apparent shear strains (γ_{xz} and γ_{yz}) measured across each fault:

$$\gamma = \frac{d}{w}$$

where d is the apparent displacement and w is the apparent width of the fault zone measured in the xz or yz plane. Then, after some trigonometry, it can be shown that:

$$\varepsilon_x = \frac{\gamma_{xz}}{\sin\beta_{xz}}\left(1 + \frac{1}{\cos\beta_{xz}}\right)$$

$$\varepsilon_y = \frac{\gamma_{yz}}{\sin\beta_{yz}}\left(1 + \frac{1}{\cos\beta_{yz}}\right)$$

$$\varepsilon_z = \frac{\gamma_{xz}}{\sin\beta_{xz}}\left(\frac{1}{\cos\beta_{xz}} - 1\right)$$

and $\beta_{xz} = \pi - 2\alpha_{xz}$, and $\beta_{yz} = \pi - 2\alpha_{yz}$.

This kinematic model of faults forming parallel to surfaces of *nfls* implies that it is the relative magnitude of the bulk principal strains and the bulk volumetric response that controls the orientations of the fault planes. It remains to be seen whether this conjectural kinematic model explains the data from field occurrences of polymodal faults, and how rock properties mediate the volumetric response, and therefore the measured failure angle, in laboratory rock deformation tests. There is scope to investigate and test a kinematic failure criterion for polymodal faulting using measured strains and volume changes.

8. Further work

8.1. Where are we now?

- There have been many observations of polymodal fault patterns, in the field and in the laboratory. Excluding the negative results from experimentalists using a Mogi-type 'degraded triaxial' apparatus, the results from experiments using three pairs of independent pistons, with careful efforts to remove frictional effects at the platens, confirm that polymodal fault patterns are produced by truly triaxial stresses in a variety of rock types (Aydin and Reches, 1982; Reches and Dieterich, 1983; Nasseri et al., 2014). Acoustic emission data recorded during shear failure plane nucleation and growth confirm the obliquity of the shear failure zone to all three principal stresses, the central role of microcracking, and possibly also micro-anticracking too (Ghaffari et al., 2014).
- The Mohr-Coulomb failure criterion, and any other failure criterion arbitrarily 'adjusted' to rule out any possible obliquity of faults to σ_2, cannot be generally applicable to triaxial deformation. The symmetry of the underlying physics – i.e. the bilateral symmetry inherent in the directional variation of the ratio of shear stress to normal stress – is inconsistent with the general case of triaxial deformation producing polymodal fault patterns. Whilst published empirical fits using truly triaxial stress laboratory tests (e.g. Reches, 1983) are able to predict stress *magnitudes* at failure, they are unable to predict the *orientations* of the faults from the stresses.
- The Healy et al. (2006a, 2006b) model of elastic interactions may be relevant for tight or crystalline rocks deforming dominantly by tensile microcracking, but is probably less relevant for porous, granular rocks deforming with a significant contribution from pore collapse and/or grain crushing (cataclasis). Assuming constant volume for the deformation of these compactive rock types is very unlikely to be valid.
- Elastoplasticity theory (e.g. Aydin et al., 2006), limit analysis (e.g. Maillot and Leroy, 2006) and work minimisation methods (e.g. Cooke and Madden, 2014) offer sound theoretical and thermodynamically valid bases to proceed. Elastoplasticity naturally incorporates volume changes and off fault deformation. However, we currently lack data on the nature and evolution of the elastoplastic constitutive tensor during polymodal faulting. Limit analysis, which can utilize elastoplasticity, and work minimization, which is independent of rheology, may provide fruitful frameworks for exploring and predicting polymodal faulting.

8.2. What do we need to move forwards?

The most pressing need is for new laboratory data from careful rock deformation experiments using truly triaxial apparatus. A key target should be the quantification of the elastoplastic constitutive tensor for different rock types, and how it evolves during the loading path (e.g. Petkovski, 2013). Furnished with these data, we can begin to approach the analysis of polymodal failure through, for example, the rigorous frameworks of elastoplasticity (critical state soil mechanics), limit analysis or work minimisation. We need more truly triaxial rock deformation experiments conducted under a range of confining pressures, loading rates and fluid pressures, all designed to explore the differences in behaviour between porous and tight rocks under truly triaxial stress. More careful analyses of the truly triaxial stress *and* strain states during deformation should now be possible, for example through the Lode parameters (Alexeev et al., 2008). Published measurements of permeability and acoustic emissions, especially their spatio-temporal evolution along the load path, would be theoretically interesting and industrially useful. A transparent programme of benchmarking and comparisons among the different types of truly triaxial apparatus – i.e. Mogi-type 'degraded triaxial' devices compared to those with three pairs of independent rams – would be hugely beneficial for the global rock mechanics community. Numerical modelling has already shown how artefacts from the Mogi-type systems might influence the nucleation – and therefore the orientation – of through-going shear fractures (Shi et al., 2011). Stress heterogeneities in the sample could also be induced by interactions between rock heterogeneity and the loading platens, as recently modelled by Pan et al. (2012).

New analogue models, building on the substantial legacy of Oertel's elegant experiments, could use modern methods such as Particle Image Velocimetry (PIV) and 3D laser scanning to map and quantify evolving patterns of strains and faults. Kaolinite + water clay cakes have been shown to possess frictional and bi-viscous rheological behaviour similar to crustal rocks (Cooke and Elst, 2012). We also need new field data from outcrops with clear assessments of contemporaneity from matrices of cross-cutting relationships and statistical analyses of central tendency, or the lack thereof, in the orientation distribution. Larger datasets from more contiguous outcrops aided by digital data acquisition would also be useful. Fault patterns mapped in high-resolution seismic reflection data could be used to produce orientation distributions of fault intersections (branch lines), for fault populations demonstrated to be coeval (through detailed stratigraphy). Polymodal and conjugate fault patterns have distinctly different branch line distributions, and these differences may become apparent in large-scale seismic datasets (Yielding, in press).

Most importantly, we need a new failure criterion or a modification to an existing one, linking stresses or strains and rock properties to polymodal fault orientations. Published failure criteria either lack the required symmetry to explain polymodal fault patterns (e.g. Mohr-Coulomb) or only predict the magnitude of the failure stress to some degree, and not the orientations of the failure planes (e.g. Reches, 1983). Development of a new theoretical framework for polymodal faulting should precede and guide the collection of more experimental data.

9. Summary

Polymodal fault patterns have been widely and repeatedly observed in the field and in the laboratory. Field examples have been found in a wide variety of lithologies, including sandstone, basalt, carbonate and gneissic basement (Donath, 1962; Aydin and Reches, 1982; Koestler and Ehrmann, 1991; Miller et al., 2007; Carvell et al., 2014). Laboratory rock deformation experiments have also produced these fault patterns in sandstone, limestone and granite (Aydin and Reches, 1982; Reches and Dieterich, 1983; Ghaffari et al., 2014; Nasseri et al., 2014). Analogue laboratory models have produced polymodal fault patterns using rock-like mixtures of clay and water (Oertel, 1965). Simple thought

experiments based on the geometry and symmetry of triaxial strain and triaxial stress remain compelling. Polymodal faulting appears to be a fundamental natural phenomenon that has potentially major implications for the patterns of fluid flow in the subsurface, the mitigation of seismic hazard and the strength anisotropy of the lithosphere. And yet our ability to predict the orientations of polymodal faults – i.e. to quantify their orientation distribution from either truly triaxial stresses or strains – remains poor.

Acknowledgements

We thank the Editors of the Journal of Structural Geology for their invitation to write this article, and for their patience while the document was produced. We also thank Ze'ev Reches and Laurel Goodwin for their thoughtful reviews that helped us to refine the key points and forced the lead author to think again about a possible kinematic model for polymodal faulting.

References

Al-Ajmi, A.M., Zimmerman, R.W., 2005. Relation between the Mogi and the Coulomb failure criteria. Int. J. Rock Mech. Min. Sci. 42 (3), 431–439.
Alexeev, A.D., Revva, V.N., Bachurin, L.L., Prokhorov, I., 2008. The effect of stress state factor on fracture of sandstones under true triaxial loading. Int. J. Fract. 149 (1), 1–10.
Anderson, E.M., 1905. The dynamics of faulting. Trans. Edinb. Geol. Soc. 8 (3), 387–402.
Angelier, J., 1991. Analyse chronologique matricielle et succession régionale des évenments tectoniques. Comptes Rendu l'Academie Sci. Paris 312, 1633–1638.
Aydin, A., Reches, Z.E., 1982. Number and orientation of fault sets in the field and in experiments. Geology 10 (2), 107–112.
Aydin, A., Borja, R.I., Eichhubl, P., 2006. Geological and mathematical framework for failure modes in granular rock. J. Struct. Geol. 28 (1), 83–98.
Beacom, L.E., Anderson, T.B., Holdsworth, R.E., 1999. Using basement-hosted clastic dykes as syn-rifting palaeostress indicators: an example from the basal Stoer Group, northwest Scotland. Geol. Mag. 136 (03), 301–310.
Bertini, G., Marcucci, M., Nevini, R., Passerini, P., Sguazzoni, G., 1985. Patterns of faulting in the Mont Blanc granite. Tectonophysics 111 (1), 65–106.
Blenkinsop, T.G., 2008. Relationships between faults, extension fractures and veins, and stress. J. Struct. Geol. 30 (5), 622–632.
Carvell, J., Blenkinsop, T., Clarke, G., Tonelli, M., 2014. Scaling, kinematics and evolution of a polymodal fault system: Hail Creek Mine, NE Australia. Tectonophysics 632, 138–150.
Chang, C., Haimson, B., 2000. True triaxial strength and deformability of the German Continental deep drilling program (KTB) deep hole amphibolite. J. Geophys. Res. Solid Earth (1978–2012) 105 (B8), 18999–19013.
Chang, C., Haimson, B., 2005. Non-dilatant deformation and failure mechanism in two Long Valley Caldera rocks under true triaxial compression. Int. J. Rock Mech. Min. Sci. 42 (3), 402–414.
Chen, W.F., 1975. Limit Analysis and Soil Plasticity. Development in Geotechnical Engineering.
Cilona, A., Baud, P., Tondi, E., Agosta, F., Vinciguerra, S., Rustichelli, A., Spiers, C.J., 2012. Deformation bands in porous carbonate grainstones: field and laboratory observations. J. Struct. Geol. 45, 137–157.
Cooke, M.L., Elst, N.J., 2012. Rheologic testing of wet kaolin reveals frictional and biviscous behavior typical of crustal materials. Geophys. Res. Lett. 39 (1).
Cooke, M.L., Madden, E.H., 2014. Is the Earth Lazy? A review of work minimization in fault evolution. J. Struct. Geol. 66, 334–346.
Crider, J.G., 2001. Oblique slip and the geometry of normal-fault linkage: mechanics and a case study from the Basin and range in Oregon. J. Struct. Geol. 23 (12), 1997–2009.
Donath, F.A., 1962. Analysis of Basin-Range structure, south-central Oregon. Geol. Soc. Am. Bull. 73 (1), 1–16.
Ekström, G., Nettles, M., Dziewoński, A.M., 2012. The global CMT project 2004–2010: centroid-moment tensors for 13,017 earthquakes. Phys. Earth Planet. Inter. 200, 1–9.
Eshelby, J.D., 1957. The determination of the elastic field of an ellipsoidal inclusion, and related problems. Proc. R. Soc. Lond. Ser. A. Math. Phys. Sci. 241 (1226), 376–396.
Eshelby, J.D., 1959. The elastic field outside an ellipsoidal inclusion. Proc. R. Soc. Lond. Ser. A, Math. Phys. Sci. 561–569.
Fisher, N.I., Lewis, T., Embleton, B.J.J., 1987. Statistical Analysis of Spherical Data. Cambridge Uni. Press, NY.
Fossen, H., Schultz, R.A., Shipton, Z.K., Mair, K., 2007. Deformation bands in sandstone: a review. J. Geol. Soc. 164 (4), 755–769.
Ghaffari, H.O., Nasseri, M.H.B., Young, R.P., 2014. Faulting of rocks in a three-dimensional stress field by micro-anticracks. Sci. Rep. 4.
Green, H.W., Young, T.E., Walker, D., Scholz, C.H., 1990. Anticrack-associated faulting at very high pressure in natural olivine. Nature 348 (6303), 720–722.
Haimson, B., 2006. True triaxial stresses and the brittle fracture of rock. In: Rock Damage and Fluid Transport, Part I, pp. 1101–1130 (Birkhäuser Basel).
Healy, D., Jones, R.R., Holdsworth, R.E., 2006a. Three-dimensional brittle shear fracturing by tensile crack interaction. Nature 439 (7072), 64–67.
Healy, D., Jones, R.R., Holdsworth, R.E., 2006b. New insights into the development of brittle shear fractures from a 3-D numerical model of microcrack interaction. Earth Planet. Sci. Lett. 249 (1), 14–28.
Healy, D., Jones, R.R., Holdsworth, R.E., 2006c. Polymodal faulting by crack or anticrack interaction. In: AGU Fall Meeting Abstracts, vol. 1, p. 0449.
Jaeger, J.C., Cook, N.G., Zimmerman, R., 2009. Fundamentals of Rock Mechanics. John Wiley & Sons.
Jamison, W.R., Stearns, D.W., 1982. Tectonic deformation of Wingate Sandstone, Colorado National Monument. AAPG Bull. 66 (12), 2584–2608.
Koestler, A.G., Ehrmann, W.U., 1991. Description of brittle extensional features in chalk on the crest of a salt ridge (NW Germany). Geol. Soc. Lond. Spec. Publ. 56 (1), 113–123.
Krantz, R.W., 1988. Multiple fault sets and three-dimensional strain: theory and application. J. Struct. Geol. 10 (3), 225–237.
Krantz, R.W., 1989. Orthorhombic fault patterns: the odd axis model and slip vector orientations. Tectonics 8 (3), 483–495.
Kwaśniewski, M., 2012. Mechanical behavior of rocks under true triaxial compression conditions—a review. True triaxial testing of rocks. CRC Press/Balkema, Leiden. 99–138.
Lisle, R.J., 1979. The representation and calculation of the deviatoric component of the geological stress tensor. J. Struct. Geol. 1 (4), 317–321.
Lisle, R.J., Orife, T.O., Arlegui, L., Liesa, C., Srivastava, D.C., 2006. Favoured states of palaeostress in the Earth's crust: evidence from fault-slip data. J. Struct. Geol. 28 (6), 1051–1066.
Lockner, D.A., Byerlee, J.D., Kuksenko, V., Ponomarev, A., Sidorin, A., 1991. Quasi-static fault growth and shear fracture energy in granite. Nature 350 (6313), 39–42.
Maillot, B., Leroy, Y.M., 2006. Kink-fold onset and development based on the maximum strength theorem. J. Mech. Phys. Solids 54 (10), 2030–2059.
Manzocchi, T., 2002. The connectivity of two-dimensional networks of spatially correlated fractures. Water Resour. Res. 38 (9), 1-1.
Mardia, K.V., Jupp, P.E., 2009. Directional Statistics. John Wiley & Sons.
Miller, J.M., Nelson, E.P., Hitzman, M., Muccilli, P., Hall, W.D.M., 2007. Orthorhombic fault–fracture patterns and non-plane strain in a synthetic transfer zone during rifting: Lennard shelf, Canning basin, Western Australia. J. Struct. Geol. 29 (6), 1002–1021.
Mitra, G., 1979. Ductile deformation zones in Blue Ridge basement rocks and estimation of finite strains. Geol. Soc. Am. Bull. 90 (10), 935–951.
Mogi, K., 1967. Effect of the intermediate principal stress on rock failure. J. Geophys. Res. 72 (20), 5117–5131.
Mogi, K., 1971a. Fracture and flow of rocks under high triaxial compression. J. Geophys. Res. 76 (5), 1255–1269.
Mogi, K., 1971b. Effect of the triaxial stress system on the failure of dolomite and limestone. Tectonophysics 11 (2), 111–127.
Morris, A., Ferrill, D.A., Henderson, D.B., 1996. Slip-tendency analysis and fault reactivation. Geology 24 (3), 275–278.
Murrell, S.A.F., Digby, P.J., 1970a. The theory of brittle fracture initiation under triaxial stress conditions—I. Geophys. J. Int. 19 (4), 309–334.
Murrell, S.A.F., Digby, P.J., 1970b. The theory of brittle fracture initiation under triaxial stress conditions—II. Geophys. J. Int. 19 (5), 499–512.
Nasseri, M.H.B., Goodfellow, S.D., Lombos, L., Young, R.P., 2014. 3-D transport and acoustic properties of Fontainebleau sandstone during true-triaxial deformation experiments. Int. J. Rock Mech. Min. Sci. 69, 1–18.
Nicol, A., Childs, C., Walsh, J.J., Schafer, K.W., 2013. A geometric model for the formation of deformation band clusters. J. Struct. Geol. 55, 21–33.
Nixon, C.W., Sanderson, D.J., Bull, J.M., 2011. Deformation within a strike-slip fault network at Westward Ho!, Devon UK: Domino vs conjugate faulting. J. Struct. Geol. 33 (5), 833–843.
Oertel, G., 1965. The mechanism of faulting in clay experiments. Tectonophysics 2 (5), 343–393.
Pan, P.Z., Feng, X.T., Hudson, J.A., 2012. The influence of the intermediate principal stress on rock failure behaviour: a numerical study. Eng. Geol. 124, 109–118.
Peacock, D.C.P., Sanderson, D.J., 1992. Effects of layering and anisotropy on fault geometry. J. Geol. Soc. 149 (5), 793–802.
Petkovski, M., 2013. Experimental detection of damage evolution in concrete under multiaxial compression. J. Eng. Mech. 139, 616–628.
Pons, A., Leroy, Y.M., 2012. Stability of accretionary wedges based on the maximum strength theorem for fluid-saturated porous media. J. Mech. Phys. Solids 60 (4), 643–664.
Potts, G.J., Reddy, S.M., 1999. Construction and systematic assessment of relative deformation histories. J. Struct. Geol. 21 (8), 1245–1253.
Ragan, D.M., 2009. Structural Geology: an Introduction to Geometrical Techniques. Cambridge University Press.
Ramsay, J.G., 1967. Folding and fracturing of rocks. McGraw-Hill Companies.
Reches, Z.E., 1978. Analysis of faulting in three-dimensional strain field. Tectonophysics 47 (1), 109–129.
Reches, Z.E., 1983. Faulting of rocks in three-dimensional strain fields II. Theoretical analysis. Tectonophysics 95 (1), 133–156.
Reches, Z.E., Dieterich, J.H., 1983. Faulting of rocks in three-dimensional strain fields I. Failure of rocks in polyaxial, servo-control experiments. Tectonophysics 95 (1), 111–132.

Reches, Z.E., Lockner, D.A., 1994. Nucleation and growth of faults in brittle rocks. J. Geophys. Res. Solid Earth (1978–2012) 99 (B9), 18159–18173.
Renner, J., Rummel, F., 1996. The effect of experimental and microstructural parameters on the transition from brittle failure to cataclastic flow of carbonate rocks. Tectonophysics 258 (1), 151–169.
Shi, L., Li, X., Bai, B., Li, Q., Feng, X., 2011. In: Kwasniewski, M., Li, X., Takahashi, M. (Eds.), Numerical Analysis of Loading Boundary Effects in Mogi-type True Triaxial Tests. CRC Press, Boca Raton, FL, pp. 19–34.
Singh, M., Raj, A., Singh, B., 2011. Modified Mohr–Coulomb criterion for non-linear triaxial and polyaxial strength of intact rocks. Int. J. Rock Mech. Min. Sci. 48 (4), 546–555.
Smith, J.V., Durney, D.W., 1992. Experimental formation of brittle structural assemblages in oblique divergence. Tectonophysics 216 (3), 235–253.
Tikoff, B., Wojtal, S.F., 1999. Displacement control of geologic structures. J. Struct. Geol. 21 (8), 959–967.
Ulusay, R., Hudson, J.A., 2012. Suggested methods for rock failure criteria: general introduction. Rock Mech. Rock Eng. 1-1.
Underhill, J.R., Woodcock, N.H., 1987. Faulting mechanisms in high-porosity sandstones; new red sandstone, Arran, Scotland. Geol. Soc. Lond. Spec. Publ. 29 (1), 91–105.
Watterson, J., 1999. The future of failure: stress or strain? J. Struct. Geol. 21 (8), 939–948.
Wessel, P., Smith, W.H., Scharroo, R., Luis, J., Wobbe, F., 2013. Generic mapping tools: Improved version released. Eos, Trans. Am. Geophys. Union 94 (45), 409–410.
Withjack, M.O., Jamison, W.R., 1986. Deformation produced by oblique rifting. Tectonophysics 126 (2), 99–124.
Woodcock, N.H., Underhill, J.R., 1987. Emplacement-related fault patterns around the Northern Granite, Arran, Scotland. Geol. Soc. Am. Bull. 98 (5), 515–527.
Yielding, G., 2015. The geometry of branch lines. In: The Geometry and Growth of Normal Faults. Geol. Soc. Lond. Spec. Publ (in press).
Zhu, W., Wong, T.F., 1997. The transition from brittle faulting to cataclastic flow: permeability evolution. J. Geophys. Res. Solid Earth (1978–2012) 102 (B2), 3027–3041.